

# Hidden Ladder in SrMoO<sub>3</sub>/SrTiO<sub>3</sub> Superlattices: Experiments and Theoretical Calculations

Hiroshi Takatsu<sup>1,\*</sup>, Naoya Yamashina<sup>1</sup>, Masayuki Ochi<sup>2</sup>, Hsin-Hui Huang<sup>3</sup>, Shunsuke Kobayashi<sup>3</sup>, Akihide Kuwabara<sup>3</sup>, Takahito Terashima<sup>4</sup>, Kazuhiko Kuroki<sup>2</sup>, and Hiroshi Kageyama<sup>1†</sup>

<sup>1</sup>*Department of Energy and Hydrocarbon Chemistry, Graduate School of Engineering, Kyoto University, Kyoto 615-8510, Japan*

<sup>2</sup>*Department of Physics, Osaka University, Machikaneyama-cho, Toyonaka, Osaka 560-0043, Japan*

<sup>3</sup>*Nanostructures Research Laboratory, Japan Fine Ceramics Center, Atsuta, Nagoya 456-8587, Japan*

<sup>4</sup>*Department of Physics, Graduate School of Science, Kyoto University, Kyoto 606-8502, Japan*

(Received December 7, 2020)

A double-layered perovskite oxide Sr<sub>3</sub>Mo<sub>2</sub>O<sub>7</sub> is considered a “hidden ladder” system with wide and narrow bands near the Fermi level, for which high- $T_c$  superconductivity is expected. However, the difficulty in synthesis, especially in the preparation of samples without oxygen deficiency, can hinder the observation of superconductivity. In this study, we constructed a double-layer SrMoO<sub>3</sub> block through artificial superlattices with the insulating SrTiO<sub>3</sub> block, (SrMoO<sub>3</sub>)<sub>m</sub>/(SrTiO<sub>3</sub>)<sub>t</sub> ( $m = 2, 4$ ;  $t = 4$ ). First-principles calculations for bilayered SrMoO<sub>3</sub> ( $m = 2$ ) exhibit a wide-narrow band structure near the Fermi level, which bears a close resemblance to Sr<sub>3</sub>Mo<sub>2</sub>O<sub>7</sub>. The dispersion along the  $k_z$  direction is strongly suppressed by increasing the number of the SrTiO<sub>3</sub> layers,  $t$ . However, no superconductivity is observed down to 0.1 K. We discuss the absence of the superconductivity for the present films on the basis of results of scanning transmission electron microscopy and band structure calculations.

arXiv:2012.02406v1 [cond-mat.str-el] 4 Dec 2020

## 1. Introduction

There has been a rapid progress in the study of unconventional iron-based superconductors.<sup>1,2)</sup> Of particular interest is the role of an incipient band - a band that does not intersect but lies close to the Fermi level. The incipient band is expected to enhance superconductivity, as suggested in heavily electron doped  $A_x\text{Fe}_{2-y}\text{Se}_2$  ( $A$  = alkali metal ions)<sup>3,4)</sup> and monolayer FeSe.<sup>5-8)</sup> Superconducting mechanisms have been discussed using finite-energy spin fluctuations.<sup>9-15)</sup> The incipient-band induced high- $T_c$  superconductivity was initially addressed in 2005 for cuprates with a ladder-type structure.<sup>16)</sup> For the two-leg ladder model with bonding and antibonding bands, one of the bands becomes wide and the other becomes narrow (or flat) once the diagonal hopping is introduced, and an interband pair-scattering process results in high- $T_c$  superconductivity. A similar idea has been extended to various quasi-one-dimensional lattice models<sup>17)</sup> as well as other lattice models.<sup>18-20)</sup>

Recently, Ogura *et al* have proposed a new type of materials that possess wide and incipient-narrow bands, bilayer Ruddlesden-Popper (RP) compounds, Sr<sub>3</sub>Mo<sub>2</sub>O<sub>7</sub> and Sr<sub>3</sub>Cr<sub>2</sub>O<sub>7</sub> (Mo<sup>4+</sup>, Cr<sup>4+</sup>,  $d^2$ ).<sup>21)</sup> Although the bilayer RP structures are apparently not ladder-shaped (Fig. 1), they have electronic structures similar to the two-leg ladder cuprate. This results from the anisotropy of the  $d_{xz}$  and  $d_{yz}$  orbitals; the  $d_{xz}$  and  $d_{yz}$  orbitals can broadly be treated separately and form the two-leg ladders along the  $x$  and  $y$  directions, respectively.<sup>21)</sup> Theoretical calculations on the basis of the fluctuation exchange approximation have shown the potential for high- $T_c$  superconductivity in this “hidden ladder” system.<sup>21)</sup>

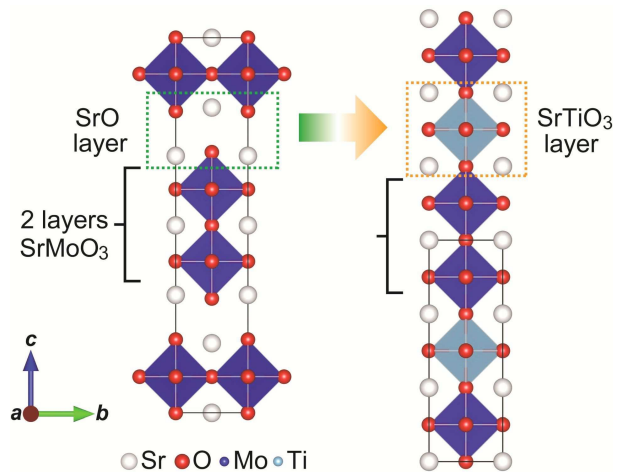


**Fig. 1.** (Color online) Crystal structures of Sr<sub>3</sub>Mo<sub>2</sub>O<sub>7</sub> and the artificial superlattice of (SrMoO<sub>3</sub>)<sub>m</sub>/(SrTiO<sub>3</sub>)<sub>t</sub> for  $(m, t) = (2, 1)$ .

Unfortunately, no sign of superconductivity has been observed experimentally in Sr<sub>3</sub>Cr<sub>2</sub>O<sub>7</sub> and Sr<sub>3</sub>Mo<sub>2</sub>O<sub>7</sub>,<sup>22,23)</sup> although the incipient band is located close to the Fermi level. For Sr<sub>3</sub>Cr<sub>2</sub>O<sub>7</sub>, orbital ordering accompanied by an antiferromagnetic order at 210 K may prevent superconductivity,<sup>22)</sup> while in the case of Sr<sub>3</sub>Mo<sub>2</sub>O<sub>7</sub>, oxygen deficiency is likely to be the main cause.<sup>21)</sup> For example, Sr<sub>3</sub>Mo<sub>2</sub>O<sub>7</sub> grown under high pressure has the oxygen content of  $\sim 6.3$ .<sup>21)</sup> Some efforts have been made to control of the partial pressure of oxygen,<sup>23,24)</sup> but it appears there remains ambiguity in the chemical composition.

Epitaxial thin film growth has an advantage for new materials synthesis in terms of rational design of ma-

\*E-mail address: takatsu@scl.kyoto-u.ac.jp

†E-mail address: kage@scl.kyoto-u.ac.jp

terials toward achieving desired properties.<sup>25–29</sup> More specifically, artificial heterostructures of functional oxides can be used as a platform to tailor their functionalities as one can modify multiple degrees of coupling between lattices, electrons, and spins and offer a controlled dimensionality. In this paper, we fabricated artificial superlattices of SrMoO<sub>3</sub> and SrTiO<sub>3</sub>, (SrMoO<sub>3</sub>)<sub>m</sub>/(SrTiO<sub>3</sub>)<sub>t</sub> ( $m = 2, 4$ ;  $t = 4$ ), with a primary motivation to realize the hidden ladder, which is the case for a double-SrMoO<sub>3</sub> block ( $m = 2$ ) (Fig. 1), where the SrTiO<sub>3</sub> block serves as an insulating block layer, instead of the SrO layers in Sr<sub>3</sub>Mo<sub>2</sub>O<sub>7</sub>. We show physical properties of the obtained films with  $m = 2$  and 4, as well as theoretical calculation of these artificial superlattices.

## 2. Calculations and Experiments

First-principles band structure calculation for (SrMoO<sub>3</sub>)<sub>m</sub>/(SrTiO<sub>3</sub>)<sub>t</sub> superlattices were performed using the WIEN2k package.<sup>30</sup> We used the Perdew-Burke-Ernzerhof parameterization of the generalized gradient approximation,<sup>31</sup> with  $RK_{\max} = 7$  and  $12 \times 12 \times k'_z$  ( $k'_z = 12/t + m$  for  $t + m \leq 4$  and  $k'_z = 2$  for  $4 < t + m$ ). For these calculations, we considered a periodic structure model (i.e., a layered oxide (SrMoO<sub>3</sub>)<sub>m</sub>(SrTiO<sub>3</sub>)<sub>t</sub> with the space group of  $P4/mmm$  (No.123) as shown in Fig. 1), assuming the ideal case of no long range orders, and optimized the structural parameters using the QUANTUM ESPRESSO package.<sup>32,33</sup>

Epitaxial films of the (SrMoO<sub>3</sub>)<sub>m</sub>/(SrTiO<sub>3</sub>)<sub>t</sub> superlattice were grown on the (001)-oriented SrTiO<sub>3</sub> or KTaO<sub>3</sub> substrate using a custom-made reactive molecular beam epitaxy (MBE) system (EGL-1420-E2, Biemtron). The films were deposited at a substrate temperature of 520 °C under O<sub>2</sub> gas flow with a background pressure of about  $4 \times 10^{-7}$  Torr. The present optimal condition was employed in the previous study on SrMoO<sub>3</sub> films with MBE.<sup>34</sup> The surface structure of the film and substrate was monitored *in-situ* by reflection high-energy electron diffraction (RHEED) with an acceleration voltage of 20 keV. Superlattices were synthesized in the following way: firstly, we estimated average interval of oscillation peaks of RHEED intensity of SrMoO<sub>3</sub> and SrTiO<sub>3</sub> at the beginning of the growth, and then we used these durations for the growth of the superlattice film.<sup>35</sup> The RHEED intensity oscillation was observed during the growth of both films, suggesting that the films were epitaxially grown in a lateral mode,<sup>25,26</sup> although the intensity decreases as the synthesis of the superlattice proceeds.

X-ray diffraction (XRD) measurements after the growth were carried out at room temperature (RT) with a Rigaku SmartLab diffractometer equipped with a Cu K $\alpha_1$  monochromator. The XRD data were analyzed by using the GlobalFit software installed in the Rigaku SmartLab XRD system. Complementary to XRD, the obtained superlattice film was also characterized by an aberration-corrected scanning transmission electron microscopy (STEM, JEM-2400FCS, JEOL Ltd.). STEM observations were performed at accelerating voltages of 200 kV. The probe-forming aperture semiangle was

22 mrad and high-angle annular dark-field (HAADF) STEM images were recorded with 68–280 mrad detectors. The cross-sectional STEM sample was prepared by dual-beam focused ion beam scanning microscopy (NB5000, Hitachi High-Technologies Co.) using Ga ions. After this treatment, Ar ion milling with a cold stage was performed. The electrical resistivity  $\rho$  was measured with a standard four-probe method. The samples were cooled down to 0.1 K using an adiabatic demagnetization refrigerator installed in a Quantum Design physical property measurement system (PPMS).

## 3. Results and discussion

### 3.1 Band structures for the (SrMoO<sub>3</sub>)<sub>m</sub>/(SrTiO<sub>3</sub>)<sub>t</sub> superlattice

In Fig. 2, we show first-principles electronic band structures of the (SrMoO<sub>3</sub>)<sub>m</sub>/(SrTiO<sub>3</sub>)<sub>t</sub> superlattice with a single-SrMoO<sub>3</sub> layer ( $m = 1$ ) or a double-SrMoO<sub>3</sub> layers ( $m = 2$ ) and insulating SrTiO<sub>3</sub> layers of different thickness ( $1 \leq t \leq 3$ ), where contributions of the Mo- $d_{xz}$  and  $d_{yz}$  orbitals are highlighted by thick lines. In the  $m = 1$  system, the Mo- $d_{xz}$  and  $d_{yz}$  orbitals form the chain-like networks along the  $x$  and  $y$  directions, respectively, which results from orbital anisotropy and the presence of insulating SrTiO<sub>3</sub> layers. The Mo- $d_{xz/yz}$  band structures for the  $m = 1$  system shown in Figs. 2(a)–(c) look similar. An important difference, however, is the  $\Gamma$ -Z dispersion (i.e., the dispersion along the  $k_z$  direction), which corresponds to the coupling among SrMoO<sub>3</sub> layers separated by SrTiO<sub>3</sub> layers. By increasing the number of the SrTiO<sub>3</sub> layers ( $t$ ), such coupling is rapidly weakened.

In the  $m = 2$  system, the Mo- $d_{xz}$  and  $d_{yz}$  orbitals in the SrMoO<sub>3</sub> bilayer form the two-leg ladders along the  $x$  and  $y$  directions, respectively. As a result, the Mo- $d_{xz/yz}$  band dispersion consists basically of the bonding and anti-bonding bands, each of which has a shape similar to the Mo- $d_{xz/yz}$  bands in the  $m = 1$  system. Here, we use the terms of bonding and anti-bonding to denote the coupling between the SrMoO<sub>3</sub> layers along the  $z$  direction. Since these two sets of the bonding and anti-bonding bands have a different bandwidth as shown in Figs. 2(d)–(f), one can say that the wide and narrow bands coexist. The same situation occurs in Sr<sub>3</sub>Mo<sub>2</sub>O<sub>7</sub>, where the  $d_{xz/yz}$  hidden ladders and the resulting coexistence of the wide and narrow bands were theoretically pointed out.<sup>21</sup> One can also see that the narrow band edge is close to the Fermi energy  $E_F$ , which results in the incipience of narrow bands similarly to Sr<sub>3</sub>Mo<sub>2</sub>O<sub>7</sub>. Because the sandwiched SrTiO<sub>3</sub> layers are insulating, the Mo- $d_{xz/yz}$  band structures in the  $m = 2$  system resemble that for Sr<sub>3</sub>Mo<sub>2</sub>O<sub>7</sub> shown in Fig. 2(g). As in the  $m = 1$  system, the  $\Gamma$ -Z dispersion in the  $m = 2$  system becomes weak with increasing  $t$ . In fact, a weaker dispersion is found in the  $(m, t) = (2, 3)$  case than Sr<sub>3</sub>Mo<sub>2</sub>O<sub>7</sub>, suggesting that the (SrMoO<sub>3</sub>)<sub>m</sub>/(SrTiO<sub>3</sub>)<sub>t</sub> superlattice with a sufficiently large  $t$  is favorable for superconductivity. Thus, (SrMoO<sub>3</sub>)<sub>m</sub>/(SrTiO<sub>3</sub>)<sub>t</sub> superlattices with  $m = 2$  are regarded as hidden two-leg ladder system that can host high- $T_c$  superconductivity even without carrier doping, as suggested by the many-body analysis of Sr<sub>3</sub>Mo<sub>2</sub>O<sub>7</sub>.<sup>21</sup> The observations shown here are somewhat reminiscent

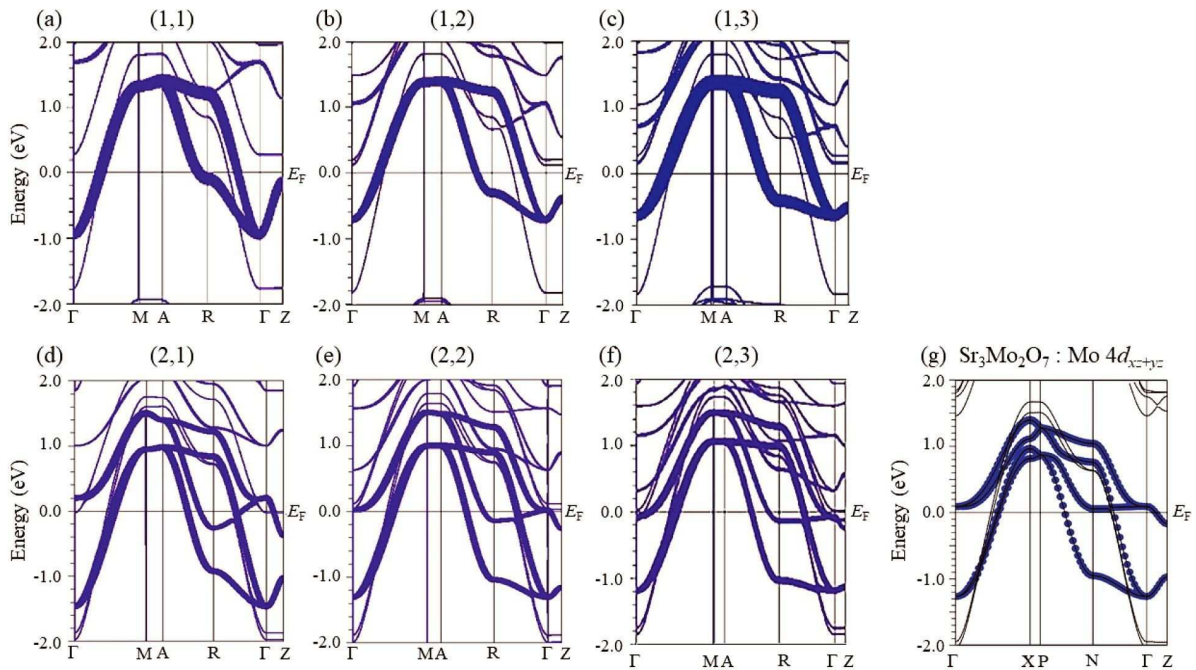


**Fig. 2.** (Color online) Band dispersions of (a)–(f)  $(\text{SrMoO}_3)_m/(\text{SrTiO}_3)_t$  for  $(m, t) = (1, 1)$ – $(1, 3)$ , and  $(m, t) = (2, 1)$ – $(2, 3)$  and (g)  $\text{Sr}_3\text{Mo}_2\text{O}_7$ , where contributions of the Mo- $d_{xz}$  and  $d_{yz}$  orbitals are highlighted to emphasize the ladder-like band. Note that symmetric points of M, A and R of  $(\text{SrMoO}_3)_m/(\text{SrTiO}_3)_t$  with the  $P4/mmm$  space group correspond to X, P, and N of  $\text{Sr}_3\text{Mo}_2\text{O}_7$  with the  $I4/mmm$  space group, respectively.

of the quantum well states in superlattices or ultra-thin films.<sup>36–38)</sup>

### 3.2 Experiments on $(m, t) = (2, 4)$ superlattice films

We initially synthesized the superlattice films of double  $\text{SrMoO}_3$  layers ( $m = 2$ ) combined with quadruple  $\text{SrTiO}_3$  layers ( $t = 4$ ) on a (001)-oriented  $\text{SrTiO}_3$  substrate. Figure 3(a) shows the out-of-plane  $\theta$ – $2\theta$  XRD pattern for the film containing eleven repetitions of the  $(m, t) = (2, 4)$  structure,  $11[(\text{SrMoO}_3)_2/(\text{SrTiO}_3)_4]$ . This film exhibits distinct satellite peaks, indicating the formation of the superlattice, although a tiny unknown peak (probably due to  $\text{MoO}_3$  related secondary phase<sup>39–41)</sup>) is present at about  $25.5^\circ$ . The experimental diffraction pattern is also deviated slightly from the calculation, based on dynamical theory of X-ray diffraction,<sup>2,3)</sup> for the ideal structure of  $11[(\text{SrMoO}_3)_2/(\text{SrTiO}_3)_4]$  (the blue solid line in Fig.3(a)).

Figure 3(b) shows the temperature dependence of the electrical resistivity  $\rho$  of the same sample. No superconductivity was observed at temperatures down to 2 K. While  $\rho$  is almost temperature independent, below 100 K it increases with decreasing temperature. Since  $\text{SrTiO}_3$  and  $\text{SrMoO}_3$  are both magnetically inactive, this increase of  $\rho$  at low temperatures is not due to the Kondo effect,<sup>44)</sup> but is ascribable to disordered-caused transport anomalies such as variable range hopping (VRH),<sup>45)</sup> weak Anderson localization (WAL),<sup>46,47)</sup> and impurity-induced electron-electron (IIEE) interaction,<sup>48)</sup> which have been observed also in films and wires.<sup>49)</sup> Owing to insulating  $d_0$  nature and large  $\rho$  of the  $\text{Mo(VI)O}_3$  related impurity phases, one can ignore their contribution to the

temperature dependence of  $\rho$ . Instead, the present result may be related to a certain disorder in the interface between  $\text{SrTiO}_3$  and  $\text{SrMoO}_3$ , which could cause the discrepancy in XRD intensity between experiment and calculation, and also account for the absence of superconductivity since superconductivity mediated by spin fluctuations tends to be affected by disorders or impurities involved in the main phase.<sup>50)</sup> The interface roughening or Ti/Mo intermixing disorder was found in STEM for the (4,4) film, which will be discussed later. Note that thick films of  $\text{SrMoO}_3$ , synthesized by the same MBE method, showed an improved  $\rho$  of  $24 \mu\Omega \text{ cm}$  at RT, as compared with the thick films by other techniques.<sup>5,51–53)</sup> On the other hand, a slight influence of extrinsic effects such as Mo(VI)-containing impurities is still seen in  $\rho$ .<sup>34)</sup> We suspect the emergence of such impurities affects the crystallinity of the heterointerface of the present superlattices, as discussed in a later section.

### 3.3 Experiments on $(m, t) = (4, 4)$ superlattice films

We examined several growth conditions for the double-layer  $\text{SrMoO}_3$  ( $m = 2$ ) films, but failed to obtain a superlattice film free from a chemical disorder around the heterointerface. Accordingly, we synthesized a superlattice film with  $(m, t) = (4, 4)$ , with a hope that the inner two  $\text{SrMoO}_3$  layers might not have chemical disorder. Although the heterointerface of the film might be disordered inevitably, we expected that such an inner double- $\text{SrMoO}_3$ -layer structure works as the hidden ladder lattice and may lead to superconductivity.

Figure 4(a) shows the out-of-plane  $\theta$ – $2\theta$  XRD pattern for the film having ten repetitions of the  $(m, t) =$

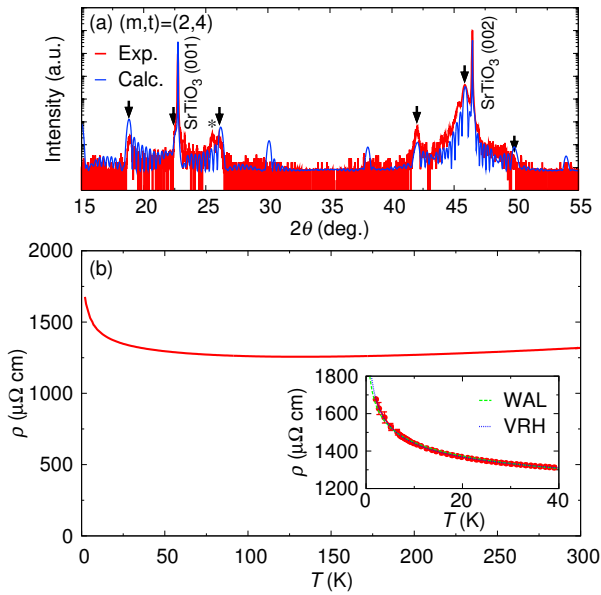


**Fig. 3.** (Color online) (a) Out-of-plane  $\theta$ - $2\theta$  XRD patterns (red line) of a  $(\text{SrMoO}_3)_m/(\text{SrTiO}_3)_t$  superlattice film on the (001)-oriented  $\text{SrTiO}_3$  substrate for  $(m, t) = (2, 4)$ . The blue line represents a dynamical theory diffraction calculation. The fundamental and satellite peaks observed are indicated by arrows. An asterisk \* represents unknown peak. (b) Temperature dependence of the electrical resistivity  $\rho$  of the same sample as (a). The inset shows the magnified view of the data plot below  $T = 40$  K, with fitting curves of WAL ( $\rho \propto \log(T)$ ) and VLH in 2D ( $\rho \propto \exp(T_0/T)^{1/d+1}$  with  $d = 2$ ). Note that the IIEE interaction also brings about logarithmic temperature dependence.<sup>48, 49</sup> These fittings imply a large influence of chemical disorder on resistivity.

(4, 4) structure,  $10[(\text{SrMoO}_3)_4/(\text{SrTiO}_3)_4]$ , grown on the (001)-oriented  $\text{SrTiO}_3$  substrate. Fundamental and superlattice satellite peaks are clearly seen. The simulated pattern for the (4, 4) structure broadly agrees with the experimental data. The same superlattice structure was also constructed on the (001)-oriented  $\text{KTaO}_3$  substrate with a similar film quality.<sup>35</sup> It is worth noting that the (4, 4) film has better quality than the (2, 4) film, which can be seen from a better match between the experimental and theoretical patterns for the former film (Figs. 3(a) and 4(a)).

STEM observations for the (4, 4) film provide detailed information on the structure, with interface roughening (Fig. 4(b)) and intermixing disorder (Figs. 4(c)-(d)) around the interface. We used the film fabricated on the  $\text{SrTiO}_3$  substrate for these experiments, since  $\rho$  is slightly lower (i.e., the quality of the film is slightly higher) than that of the film on the  $\text{KTaO}_3$  substrate, as discussed in a later section. The roughness and site exchange around the interface between  $\text{SrMoO}_3$  and  $\text{SrTiO}_3$  films would primarily be ascribed to a poorer crystallinity of  $\text{SrMoO}_3$  vs.  $\text{SrTiO}_3$ . An insulating Mo(VI)-containing impurity, which often appears in  $\text{SrMoO}_3$  films,<sup>4-6</sup> may affect the crystallinity of  $\text{SrMoO}_3$ . STEM measurements revealed trace impurity with a structure different from perovskites.<sup>35</sup> Interface roughening could also result from the lattice mismatch between  $\text{SrMoO}_3$  ( $a = 3.976$  Å)<sup>57</sup> and  $\text{SrTiO}_3$  ( $a = 3.905$  Å).<sup>58</sup> Additionally, the differ-

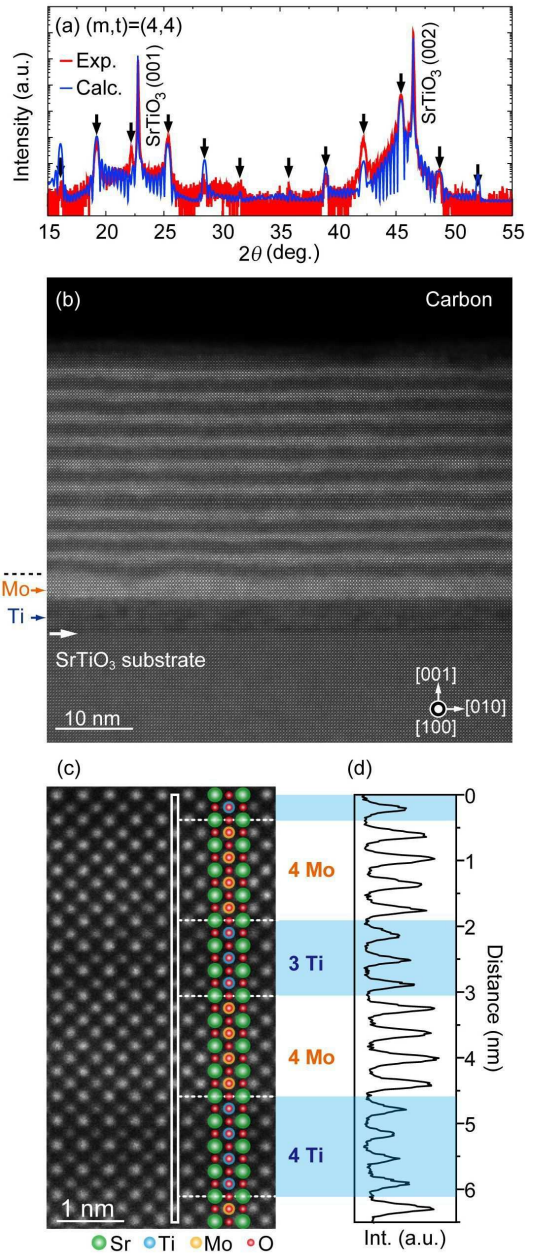


**Fig. 4.** (Color online) (a) Out-of-plane  $\theta$ - $2\theta$  XRD patterns of a  $(\text{SrMoO}_3)_m/(\text{SrTiO}_3)_t$  superlattice film on the (001)-oriented  $\text{SrTiO}_3$  substrate for  $(m, t) = (4, 4)$ . The blue line represents a dynamical theory diffraction calculation. The fundamental and satellite peaks are indicated by arrows. A peak at about  $22.5^\circ$  is a superlattice peak, not due to an impurity secondary phase, although it is slightly deviated from the calculation. (b) HAADF STEM image of the  $\text{SrMoO}_3/\text{SrTiO}_3$  superlattice film taken from the [100] zone axis of the  $\text{SrTiO}_3$  substrate. The same sample as (a) was used for this experiment. The white arrow indicates the interface between substrate and superlattice film. (c) Magnified view of the HAADF STEM image of the superlattice and (d) the intensity profile of B-site cation (Ti or Mo) columns obtained from the white rectangle region in (c).

ence in surface energies between  $\text{SrMoO}_3$  and  $\text{SrTiO}_3$  films may be at play, which has been suggested in  $\text{EuMoO}_3/\text{SrTiO}_3$  superlattices.<sup>59</sup>

Although the heterointerface of the (4, 4) film is disordered, the inner two layers of the quadruple  $\text{SrMoO}_3$  layers look clean (Figs. 4(b)-(c)). Using this

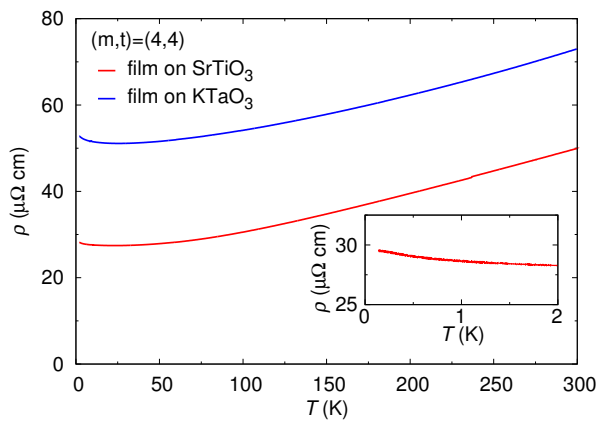


**Fig. 5.** (Color online) Temperature dependence of the electrical resistivity  $\rho$  of the same film as Fig. 4(a) on the (001)-oriented SrTiO<sub>3</sub> substrate and the (4, 4) film on the (001)-oriented KTaO<sub>3</sub> substrate. The slight enhancement of  $\rho$  in the film on the KTaO<sub>3</sub> substrate could be attributed to enhanced impurity scattering around roughened interfaces. The inset shows the low-temperature behavior of  $\rho$  of the film on the SrTiO<sub>3</sub> substrate.

film, we measured the temperature dependence of  $\rho$ , the result of which is shown in Fig. 5, along with a 10[(SrMoO<sub>3</sub>)<sub>4</sub>/(SrTiO<sub>3</sub>)<sub>4</sub>] film on the KTaO<sub>3</sub> substrate. Both films exhibit metallic temperature dependence with a positive slope ( $d\rho/dT > 0$ ), as opposed to the (2, 4) film (Fig. 3(b)). The slight enhancement of  $\rho$  is seen in the film on the KTaO<sub>3</sub> substrate, probably due to the enhancement of impurity scattering. There may be some effect of the epitaxial tensile strain from the KTaO<sub>3</sub> substrate, the actual effect of which is not clear in physical properties of the film obtained. On the other hand, it is noteworthy that  $\rho$  of both films on the SrTiO<sub>3</sub> and KTaO<sub>3</sub> substrates is much lower (about 30 times smaller) than that of the (2, 4) film. This result implies that charge carriers in the (4, 4) film mainly move through the inner bilayers; i.e., the influence of impurities or disorder is small in the inner bilayers. However, no superconductivity nor any signature of magnetic phase transitions were observed down to 0.1 K (the inset of Fig. 5).

### 3.4 Band structure calculation for the $(m, t) = (4, 4)$ superlattice and the absence of superconductivity

We performed first-principles band structure calculations for the disorder-free (4, 4) superlattice. Here, we separately examine the contributions from the inner and outer bilayers (Fig. 6(a)). Figures 6(b) and (c) show the band structure, where contributions of the Mo- $d_{xz}/d_{yz}$  orbitals in the inner and outer layers are highlighted by thick lines, respectively. Notably, the narrow band of the inner bilayers is far away from  $E_F$  (Fig. 6(b)) and hence may not function as an incipient band that contributes to the enhanced superconductivity. On the other hand, the band of the outer layers sits close to  $E_F$  (Fig. 6(c)) and can work as an incipient band. It is thus possible that the superconducting correlation is suppressed in the superlattice with  $m = 4$  in the presence of disorder at the heterointerface. Oxygen deficiency, discussed in the previous theoretical study,<sup>21)</sup> is also a possible origin for the

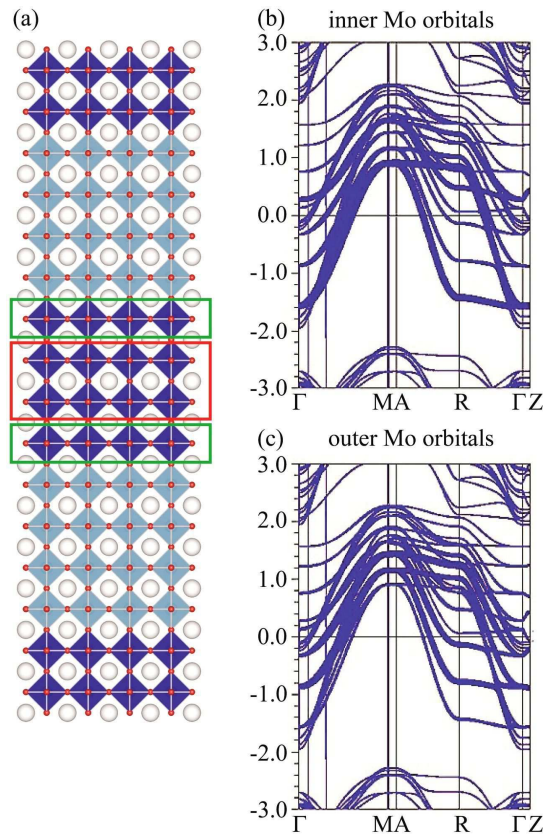


**Fig. 6.** (Color online) (a) Crystal structure of (SrMoO<sub>3</sub>)<sub>4</sub>/(SrTiO<sub>3</sub>)<sub>4</sub> and (b,c) its band structure, where the Mo- $d_{xz}/d_{yz}$  orbital weight in the inner and outer layers is highlighted, respectively. The inner and outer SrMoO<sub>3</sub> layers are shown by the red and green squares in (a), respectively.

absence of superconductivity.

Although superconductivity was not observed, this study has clearly demonstrated that electronic structures similar to a naturally available Sr<sub>3</sub>Mo<sub>2</sub>O<sub>7</sub> (and cuprate ladders) can be obtained simply by constructing artificial superlattice of perovskite SrMoO<sub>3</sub> and SrTiO<sub>3</sub>, with a further room for modification of electronic structures by changing a repetition of stacking sequence. The present system is in a sense analogous to the quantum well structure of perovskites studied in ultra-thin films;<sup>36)</sup> SrVO<sub>3</sub> with the  $d^1$  configuration exhibits a metal insulator transition at a critical thickness of 2–3 layers through a pseudogap region with a thickness below 6 layers.<sup>60)</sup> Thus electron doping to the insulator phase could be achieved by using SrMoO<sub>3</sub> with the  $d^2$  configuration.

## 4. Conclusion

We have fabricated the superlattice of SrMoO<sub>3</sub> and SrTiO<sub>3</sub>, (SrMoO<sub>3</sub>)<sub>m</sub>/(SrTiO<sub>3</sub>)<sub>t</sub>, inspired by the recent theoretical prediction of superconductivity in the bilayer RP compound Sr<sub>3</sub>Mo<sub>2</sub>O<sub>7</sub>. First-principles calculations for (SrMoO<sub>3</sub>)<sub>2</sub>(SrTiO<sub>3</sub>)<sub>t</sub> ( $t \geq 2$ ) show similar characteristics with Sr<sub>3</sub>Mo<sub>2</sub>O<sub>7</sub>, which features a ladder-like electronic band structure with wide and narrow bands, suggesting a potential high- $T_c$  superconductivity in this artificial superlattice. Experimentally, we have succeeded in growing the superlattices with  $(m, t) = (2, 4)$  and  $(4, 4)$ .

The absence of superconductivity in our films might be due to a chemical disorder in the interface. Further optimization of growth conditions is essential to reduce interface roughening and/or intermixing disorder. Such a superlattice with SrMoO<sub>3</sub> is also an interesting future topic as quantum well structures.

### Acknowledgment

This work was supported by CREST (JP-MJCR1421) and JSPS KAKENHI Grants (No. JP16H06439, No. JP16H06440, No. JP17H04849, No. JP17H05481, No. JP18H01860, No. JP18K13470, and No. JP19H04697).

- 1) H. Hosono and K. Kuroki: *Physica C* **514** (2015) 399.
- 2) A. Chubukov and P. J. Hirschfeld: *Physics Today* **68** (2015) 46.
- 3) J. Guo, S. Jin, G. Wang, S. Wang, K. Zhu, T. Z. M. He, and X. Chen: *Phys. Rev. B* **82** (2010) 180520.
- 4) M. H. Fang, H. D. Wang, C.-H. Dong, Z. J. Li, C. M. Feng, J. Chen, and H. Q. Yuan: *Europhys. Lett.* **94** (2011) 27009.
- 5) Q. Y. Wang, Z. Li, W. H. Zhang, Z. C. Zhang, J. S. Zhang, W. Li, H. Ding, Y. B. Ou, P. Deng, K. Chang, J. Wen, C. L. Song, K. He, J. F. Jia, S. H. Ji, Y. Wang, L. Wang, X. Chen, X. Ma, , and Q. K. Xue: *Chin. Phys. Lett.* **29** (2012) 037402.
- 6) D. Liu, W. Zhang, D. Mou, J. He, Y. B. Ou, Q. Y. Wang, Z. Li, L. Wang, L. Zhao, S. He, Y. Peng, X. Liu, C. Chen, L. Yu, G. Liu, X. Dong, J. Zhang, C. Chen, Z. Xu, J. Hu, X. Chen, X. Ma, Q. Xue, and X. J. Zhou: *Nat. Commun.* **2** (2012) 931.
- 7) J. F. Ge, Z. L. Liu, C. Liu, C. L. Gao, D. Qian, Q. K. Xue, Y. Liu, and J. F. Jia: *Nat. Mater.* **14** (2015) 285.
- 8) J. Shiogai, Y. Ito, T. Mitsuhashi, T. Nojima, and A. Tsukazaki: *Nat. Phys.* **12** (2016) 42.
- 9) P. J. Hirschfeld, M. M. Korshunov, and I. I. Mazin: *Rep. Prog. Phys.* **74** (2011) 124508.
- 10) F. Wang, F. Yang, M. Gao, Z. Y. Lu, T. Xiang, and D. H. Lee: *Europhys. Lett.* **93** (2011) 57003.
- 11) Y. Bang: *New J. Phys.* **16** (2014) 023029.
- 12) X. Chen, S. Maiti, A. Linscheid, and P. J. Hirschfeld: *Phys. Rev. B* **92** (2015) 224514.
- 13) Y. Bang: *New J. Phys.* **18** (2016) 113054.
- 14) V. Mishra, D. J. Scalapino, and T. A. Maier: *Sci. Rep.* **6** (2016) 32078.
- 15) V. Mishra, D. J. Scalapino, and T. A. Maier: *Phys. Rev. B* **99** (2019) 140504(R).
- 16) K. Kuroki, T. Higashida, and R. Arita: *Phys. Rev. B* **72** (2005) 212509.
- 17) K. Matsumoto, D. Ogura, and K. Kuroki: *Phys. Rev. B* **97** (2018) 014516.
- 18) K. Kobayashi, M. Okumura, S. Yamada, M. Machida, and H. Aoki: *Phys. Rev. B* **94** (2016) 214501.
- 19) M. Nakata, D. Ogura, H. Usui, and K. Kuroki: *Phys. Rev. B* **95** (2017) 214509.
- 20) T. Misumi and H. Aoki: *Phys. Rev. B* **96** (2017) 155137.
- 21) D. Ogura, H. Aoki, and K. Kuroki: *Phys. Rev. B* **96** (2017) 184513.
- 22) J. Jeanneau, P. Toulemonde, G. Remenyi, A. Sulpice, C. Colin, V. Nassif, E. Suard, E. S. Colera, G. R. Castro, F. Gay, C. Urdaniz, R. Weht, C. Fevrier, A. Ralko, C. Lacroix, A. A. Aligia, and M. Núñez-Regueiro: *Phys. Rev. Lett.* **118** (2017) 207207.
- 23) S. Kouno, N. Shirakawa, I. Nagai, N. Umeyama, K. Tokiwa, and T. Watanabe: *J. Phys. Soc. Jpn.* **76** (2007) 094706.
- 24) U. Steiner and W. Reichelt: *Z. Naturforsch. B* **53** (1998) 110.
- 25) G. Koster, M. Huijben, and G. Rijnders: *Epitaxial Growth of Complex Metal Oxides* (Woodhead Publishing, UK, 2015).
- 26) J. R. Arthur: *Surface Science* **500** (2002) 189.
- 27) O. Y. Gorbenko, S. V. Samoilenkov, I. E. Graboy, and A. R. Kaul: *Chem. Mater* **14** (2002) 4026.
- 28) D. G. Schlom, L.-Q. Chen, X. Pan, A. Schmehl, and M. A. Zurbuchen: *J. Am. Ceram. Soc.* **91** (2008) 2429.
- 29) D. Oka and T. Fukumura: *CrystEngComm* **19** (2017) 2144.
- 30) P. Blaha, K. Schwarz, G.K.H. Madsen, D. Kvasnicka, J. Luitz, WIEN2k, An Augmented Plane Wave Plus Local Orbitals Program For Calculating Crystal Properties, Vienna University of Technology, Austria, 2001.
- 31) J. P. Perdew, K. Burke, and M. Ernzerhof: *Phys. Rev. Lett.* **77** (1996) 3865.
- 32) P. Giannozzi, S. Baroni, N. Bonini, M. Calandra, R. Car, C. Cavazzoni, D. Ceresoli, G. L. Chiarotti, M. Cococcioni, and I. Dabo: *Journal of Physics: Condensed Matter* **21** (2009) 395502.
- 33) P. Giannozzi, O. Andreussi, T. Brumme, O. Bunau, M. B. Nardelli, M. Calandra, R. Car, C. Cavazzoni, D. Ceresoli, and M. Cococcioni: *Journal of Physics: Condensed Matter* **29** (2017) 465901.
- 34) H. Takatsuet *al.*: to be published in *J. Cryst. Growth* .
- 35) Supplemental Material of this paper for the RHEED intensity oscillation during the growth of the (SrMoO<sub>3</sub>)<sub>m</sub>/(SrTiO<sub>3</sub>)<sub>t</sub> superlattice film, XRD results and analysis of the superlattice film on the KTaO<sub>3</sub> substrate, and additional STEM data.
- 36) K. Yoshimatsu, K. Horiba, H. Kumigashira, T. Yoshida, A. Fujimori, and M. Oshima: *Science* **333** (2011) 319.
- 37) A. V. Boris, Y. Matiks, E. Benckiser, A. Frano, P. Popovich, V. Hinkov, P. Wochner, M. Castro-Colin, E. Detemple, V. K. Malik, C. Bernhard, T. Prokscha, A. Suter, Z. Salman, E. Morenzoni, G. Cristiani, H. U. Habermeier, and B. Keimer: *Science* **332** (2011) 937.
- 38) L. Esaki and R. Tsu: *IBM J. Res. Develop.* **14** (1970) 61.
- 39) A. Magnéli: *Acta Chem. Scand.* **2** (1948) 501.
- 40) M. Sato, M. Onoda, and Y. Matsuda: *J. Phys. C: Solid State Phys.* **20** (1987) 4763.
- 41) J. B. Parise, E. M. M. III, R. V. Dreele, and J. A. ColdStone: *J. Solid State Chem.* **93** (1991) 193.
- 42) T. Takahashi and S. Nakatani: *Surface Science* **326** (1995) 347.
- 43) W. Yashiro, Y. Ito, M. Takahasi, and T. Takahashi: *Surface Science* **490** (2001) 394.
- 44) J. Kondo: *Proc. Theor. Phys.* **32** (1964) 37.
- 45) N. F. Mott: *Philosophical Magazine* **19** (1968) 835.
- 46) E. Abrahams, P. W. Anderson, D. C. Licciardello, and T. V. Ramakrishnan: *Phys. Rev. Lett.* **42** (1979) 673.
- 47) P. W. Anderson, E. Abrahams, and T. V. Ramakrishnan: *Phys. Rev. Lett.* **43** (1979) 718.
- 48) B. L. Altshuler, A. G. Aronov, and P. A. Lee: *Phys. Rev. Lett.* **44** (1980) 1288.
- 49) P. A. Lee and T. V. Ramakrishnan: *Rev. Mod. Phys.* **57** (1985) 287.
- 50) J. M. Tarascon, L. H. Greene, P. Barboux, W. R. McKinnon, G. W. Hull, T. P. Orlando, K. A. Delin, S. Foner, and E. J. McNiff: *Phys. Rev. B* **36** (1987) 8393.
- 51) T. Inukai and T. Murakami: *J. J. Appl. Phys.* **24** (1985) 21.
- 52) H. H. Wanga, D. F. Cui, Y. L. Zhou, Z. H. Chena, F. Chena, T. Zhao, H. B. L. G. Z. Yanga, M. C. Xub, Y. C. Lanb, X. L. Chenb, H. J. Qianc, and F. Q. Liuc: *J. Cryst. Growth* **226** (2001) 261.
- 53) A. Radetinac, K. S. Takahashi, L. Alff, M. Kawasaki, and Y. Tokura: *Appl. Phys. Express* **3** (2010) 073003.
- 54) A. Radetinac, J. Zimmermann, K. Hoyer, H. Zhang, P. Komissinskiy, and L. Alffa: *J. Appl. Phys.* **119** (2016) 055302.
- 55) H. Wadati, J. Mravlje, K. Yoshimatsu, H. Kumigashira, M. Oshima, T. Sugiyama, E. Ikenaga, A. Fujimori, A. Georges, A. Radetinac, K. S. Takahashi, M. Kawasaki, and Y. Tokura: *Phys. Rev. B* **90** (2014) 205131.
- 56) P. Salg, D. Walk, L. Zeinar, A. Radetinac, L. Molina-Luna, A. Zintler, R. Jakoby, H. Maune, P. Komissinskiy, and L. Alff: *APL Mater.* **7** (2019) 051107.
- 57) R. B. Macquart, B. J. Kennedy, and M. Avdeev: *J Solid State Chem.* **183** (2010) 249.

- 58) M. Schmidbauer, A. Kwasniewski, and J. Schwarzkopf: *Acta Cryst. B* **68** (2012) 8.
- 59) T. C. Fujita, Y. Kozuka, H. Seki, and M. Kawasaki: *Phys. Rev. B* **87** (2013) 205402.
- 60) K. Yoshimatsu, T. Okabe, H. Kumigashira, S. Okamoto, S. Aizaki, A. Fujimori, and M. Oshima: *Phys. Rev. Lett.* **104** (2010) 147601.

## Supplements for “Hidden Ladder in SrMoO<sub>3</sub>/SrTiO<sub>3</sub> Superlattices: Experiments and Theoretical Calculations”

### Abstract

In this supplemental material, we show experimental results of the high-energy electron diffraction (RHEED) intensity oscillation during the growth of a superlattice film, X-ray diffraction (XRD) data of a (SrMoO<sub>3</sub>)<sub>4</sub>/(SrTiO<sub>3</sub>)<sub>4</sub> film on the KTaO<sub>3</sub> substrate, additional data of scanning transmission electron microscopy (STEM) for a superlattice film.

### RHEED intensity oscillation

Figure S1 shows one of the typical results of RHEED intensity oscillation during the growth of superlattice film of (SrMoO<sub>3</sub>)<sub>4</sub>/(SrTiO<sub>3</sub>)<sub>4</sub> on the (001)-oriented SrTiO<sub>3</sub> substrate. At the beginning of the film growth (pre-growth), we estimated the average time of the interval of oscillation peaks, since the interval corresponds to the growth of one unit cell of SrMoO<sub>3</sub> (or SrTiO<sub>3</sub>).<sup>1)</sup> We often observed that the RHEED intensity decreases when switching from the growth of SrTiO<sub>3</sub> to that of SrMoO<sub>3</sub>. This behavior is probably due to the emergence of interface roughening or disorder around the heterointerface, both of which were detected by STEM experiments. However, the intensity oscillations can be maintained to the end of the growth. Therefore, we utilized this behavior for the growth of the superlattice, i.e., each layer thickness was controlled by *in-situ* monitoring of the intensity oscillation in addition to the use of the averaged time of the oscillation interval.

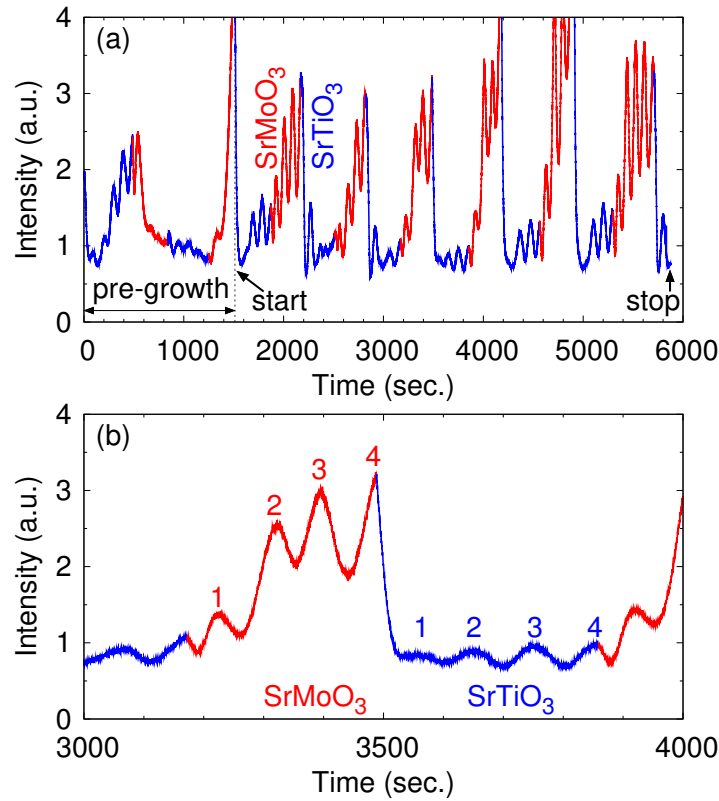


**Fig. S1.** (a) RHEED intensity oscillations during the growth of (SrMoO<sub>3</sub>)<sub>m</sub>/(SrTiO<sub>3</sub>)<sub>t</sub> with  $(m, t) = (4, 4)$ . (b) Magnified view of the intensity of the RHEED oscillation, shown in (a).

### XRD results of a (SrMoO<sub>3</sub>)<sub>4</sub>/(SrTiO<sub>3</sub>)<sub>4</sub> film on the KTaO<sub>3</sub> substrate

Figure S2 shows the  $\theta$ - $2\theta$  XRD scan of a (SrMoO<sub>3</sub>)<sub>m</sub>/(SrTiO<sub>3</sub>)<sub>t</sub> film on the (001)-oriented KTaO<sub>3</sub> substrate. The film has ten repetitions of the  $(m, t) = (4, 4)$  structure, 10[(SrMoO<sub>3</sub>)<sub>4</sub>/(SrTiO<sub>3</sub>)<sub>4</sub>], as similar to the film on the SrTiO<sub>3</sub> substrate, shown in Fig. 4 in the main text. Fundamental and superlattice satellite peaks are clearly seen. The simulated pattern for the  $(4, 4)$  structure agrees with the experimental results, suggesting that the quality of the film is good within the confirmation of the XRD level. The electrical resistivity  $\rho$  of this film is shown in Fig. 5 of the main text.



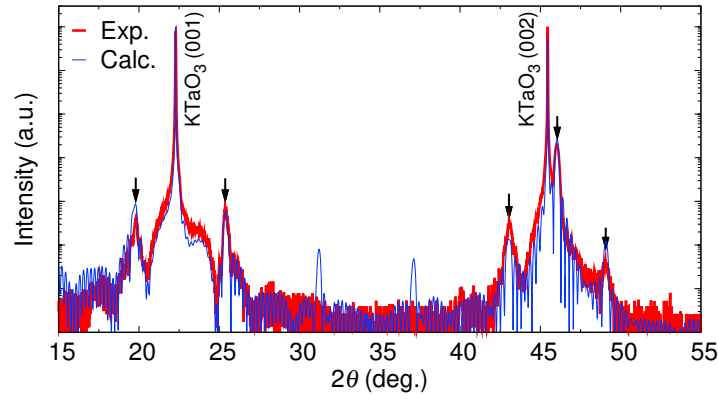


**Fig. S2.** Out-of-plane  $\theta$ - $2\theta$  XRD patterns of a film of  $10[(\text{SrMoO}_3)_4/(\text{SrTiO}_3)_4]$  on the (001)-oriented  $\text{KTaO}_3$  substrate. The blue line represents a dynamical theory diffraction calculation<sup>2,3)</sup> for the ideal structure of  $10[(\text{SrMoO}_3)_4/(\text{SrTiO}_3)_4]$ . The fundamental and satellite peaks observed are indicated by arrows.

### Magnified view of the STEM image of $(\text{SrMoO}_3)_4/(\text{SrTiO}_3)_4$

In Fig. S3, we present the magnified view of the high-angle annular dark-field (HAADF) STEM image of a superlattice film of  $10[(\text{SrMoO}_3)_4/(\text{SrTiO}_3)_4]$  on the  $\text{SrTiO}_3$  substrate. The sample is the same as that shown in Fig. 4 of the main text. We found another crystalline phase, as indicated by the arrow in Fig. S3, in the surface of the  $\text{SrMoO}_3$  film or interface between the  $\text{SrMoO}_3$  and  $\text{SrTiO}_3$  films. The structure of this additional phase is different from the perovskite structure, and the amount is minute, which was clarified by increasing contrast of the image. The presence of such a impurity may affect the crystallinity of  $\text{SrMoO}_3$  around the heterointerface with  $\text{SrTiO}_3$ , resulting in interface roughing or intermixing disorder. It is known that an impurity phase with the  $\text{Mo}^{6+}$  valence state is often observed in the growth of  $\text{SrMoO}_3$  films.<sup>4-6)</sup>

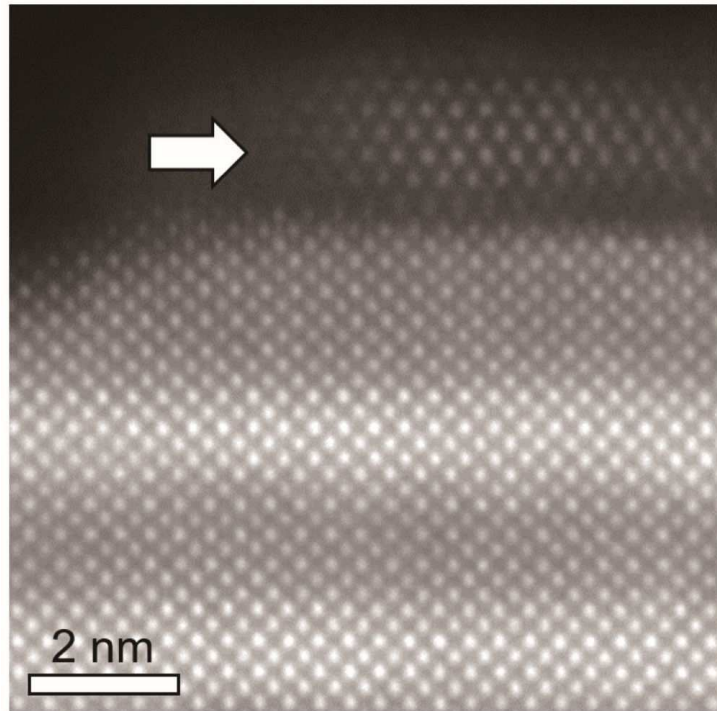


**Fig. S3.** Magnified view of the high resolution HAADF-STEM image of the  $(\text{SrMoO}_3)_4/(\text{SrTiO}_3)_4$  superlattice, fabricated on the (001)-oriented  $\text{SrTiO}_3$  substrate.

## References

- 1) T. Terashima, Y. Bando, K. Iijima, K. Yamamoto, K. Hirata, K. Hayashi, K. Kamigaki, and H. Terauchi: Phys. Rev. Lett. **65** (1990) 2684.
- 2) T. Takahashi and S. Nakatani: Surface Science **326** (1995) 347.
- 3) W. Yashiro, Y. Ito, M. Takahasi, and T. Takahashi: Surface Science **490** (2001) 394.
- 4) H. Wadati, J. Mravlje, K. Yoshimatsu, H. Kumigashira, M. Oshima, T. Sugiyama, E. Ikenaga, A. Fujimori, A. Georges, A. Radetinac, K. S. Takahashi, M. Kawasaki, and Y. Tokura: Phys. Rev. B **90** (2014) 205131.
- 5) A. Radetinac, J. Zimmermann, K. Hoyer, H. Zhang, P. Komissinskiy, and L. Alff: J. Appl. Phys. **119** (2016) 055302.
- 6) P. Salg, D. Walk, L. Zeinar, A. Radetinac, L. Molina-Luna, A. Zintler, R. Jakoby, H. Maune, P. Komissinskiy, and L. Alff: APL Mater. **7** (2019) 051107.